PHOTOSYNTHESIS

Structural adaptations of photosynthetic complex I enable ferredoxin-dependent electron transfer

Jan M. Schuller[1]*, James A. Birrell[2], Hideaki Tanaka[3,4], Tsuyoshi Konuma[5], Hannes Wulfhorst[6,7]†, Nicholas Cox[2,8], Sandra K. Schuller[9], Jacqueline Thiemann[6], Wolfgang Lubitz[2], Pierre Sétif[10], Takahisa Ikegami[5], Benjamin D. Engel[11], Genji Kurisu[3,4]*, Marc M. Nowaczyk[6]*

Photosynthetic complex I enables cyclic electron flow around photosystem I, a regulatory mechanism for photosynthetic energy conversion. We report a 3.3-angstrom-resolution cryo−electron microscopy structure of photosynthetic complex I from the cyanobacterium *Thermosynechococcus elongatus*. The model reveals structural adaptations that facilitate binding and electron transfer from the photosynthetic electron carrier ferredoxin. By mimicking cyclic electron flow with isolated components in vitro, we demonstrate that ferredoxin directly mediates electron transfer between photosystem I and complex I, instead of using intermediates such as NADPH (the reduced form of nicotinamide adenine dinucleotide phosphate). A large rate constant for association of ferredoxin to complex I indicates efficient recognition, with the protein subunit NdhS being the key component in this process.

Two light-driven electron transport pathways operate in all organisms that perform oxygenic photosynthesis: linear and cyclic electron flow. In linear electron flow (LEF), two photochemical reaction centers (photosystems I and II) act in series to drive the synthesis of adenosine triphosphate (ATP) and the reduced form of nicotinamide adenine dinucleotide phosphate (NADPH), whereas cyclic electron flow (CEF), powered by only photosystem I (PSI), leads solely to the formation of ATP. The contribution of each pathway varies in response to the environment (e.g., light quality), and organisms in which CEF is inactivated are functionally impaired (*1*).

Photosynthetic complex I of plant chloroplasts and cyanobacteria (*2*, *3*) has been implicated in CEF, taking electrons from and indirectly reinjecting them into PSI. It is structurally and functionally related to respiratory complex I from mitochondria and bacteria (*4*–*6*), but it lacks the peripheral dehydrogenase module (N-module), comprising subunits NuoE, NuoF, and NuoG (see table S1 for nomenclature in different organisms). This module catalyzes NADH (the reduced form of nicotinamide adenine dinucleotide) oxidation and contains five out of eight iron-sulfur (Fe-S) clusters. Biochemical and proteomic analyses of photosynthetic complexes have discovered at least eight distinct subunits required to assemble fully functional photosynthetic complex I (*7*–*13*). There is evidence that ferredoxin (Fd) likely mediates electron transfer between photosynthetic complex I and PSI (*14*), probably within a large supercomplex (*15*), but this process has not been directly observed. Furthermore, the structural adaptions that enable the photosynthetic complex to perform its distinct role remain uncharacterized.

We purified photosynthetic complex I from the thermophilic cyanobacterium *Thermosynechococcus elongatus* (fig. S1 and tables S2 and S3) and determined the structure by cryo–electron microscopy (cryo-EM) single-particle analysis to an overall resolution of 3.3 Å (Fig. 1; figs. S2 and S3; and table S4). We constructed models from homologous subunits or de novo where no model was available (fig. S4), except for NdhV, which binds transiently (*7*) and was not observed.

Photosynthetic complex I transfers electrons to the terminal acceptor plastoquinone. The quinone-binding site is coupled to the proton-pumping machinery in the membrane by a highly conserved charge-redistribution cascade (figs. S5 and S6), but the exact coupling mechanism remains elusive (*16*–*19*).

The photosynthesis-specific single-spanning membrane proteins NdhQ and NdhP (*8*) bind to either side of the NdhD protein, with NdhQ fixing the very long horizontal helix of NdhF (fig. S7). NdhP forms a small hydrophobic cavity to which a molecule of β-carotene is bound. A lipid molecule (monogalactosyldiacylglycerol) binds between the NdhD and NdhF proton channels and appears to be stabilized by the β-carotene molecule. Both molecules probably serve as "molecular glue," similar to lipids found in complex I of other species (*18*, *20*), to help assemble the proton-pumping membrane arm of the complex and to stabilize the NdhF binding interface. A third photosynthesis-specific membrane subunit, NdhL, binds to the N terminus of NdhA to form an extended heel under the peripheral arm (fig. S5).

The N-module subunits responsible for NADH oxidation are not present in photosynthetic complex I. Instead, the peripheral arm of the cyanobacterial complex (Q-module) contains photosynthesis-specific subunits (NdhM, NdhN, NdhO, and NdhS) (figs. S8 and S9), which bind to the conserved, nonmembrane subunits of complex I (NdhH, NdhI, NdhJ, and NdhK). The latter four subunits harbor three [4Fe-4S] clusters in addition to the quinone-binding site and have elongated termini that are conserved within the green linage (figs. S10 to S12). NdhM and NdhN are located at one side of the peripheral arm and form multiple interactions with the conserved [4Fe-4S]-carrying complex I subunits by binding to their elongated termini and covering otherwise solvent-exposed hydrophobic patches. NdhO has a globular fold and packs tightly to the side of NdhJ via a hydrophobic binding interface, covering the same space that is occupied by the species-specific protein TTHA1528 in *T. thermophilus* respiratory complex I (*21*). Furthermore, the photosynthesis-specific NdhS subunit, previously implicated in Fd binding (*22*), is located in a V-shaped groove formed by the NdhI protein, at a similar location to subunit Nqo15 within the N-module.

Our cryo-EM structure resolves the positions and conserved coordination of three [4Fe-4S] clusters, corresponding to the previously identified clusters N6a, N6b, and N2 in respiratory complex I (Fig. 2A). Electron paramagnetic resonance (EPR) measurements on chemically reduced samples quantitatively identify all three clusters (components 1, 2, and 3 in Fig. 2B). Components 1 and 2 are similar to the respiratory complex I signals of N2 and N6b (*23*, *24*), whereas component 3 bears little resemblance to N6a, in terms of width and structure (tables S6 and S13). The difference is due to either the proximity of N6a to N6b or the fact that N6a is surface exposed in photosynthetic complex I, as opposed to being buried in the protein, allowing it to act as the site of electron injection (see supplementary text).

To test the hypothesis that reduced Fd can inject electrons into photosynthetic complex I to enable CEF, we used absorption kinetics in
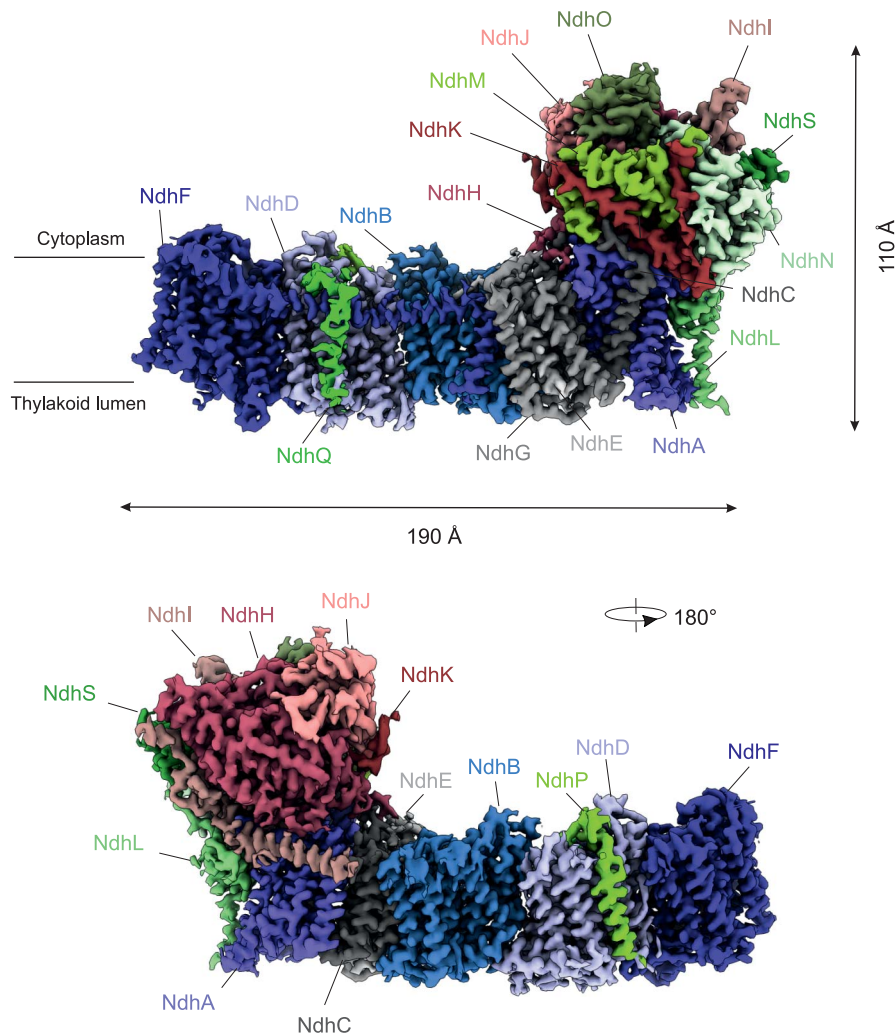
Fig. 1. Cryo-EM map of photosynthetic complex I from *T. elongatus* segmented by subunit. Eighteen subunits are colored and named accordingly (photosynthesis-specific subunits NdhL, NdhM, NdhN, NdhO, NdhP, NdhQ, and NdhS; other nonmembrane subunits NdhH, NdhI, NdhJ, and NdhK; and other membrane subunits NdhA, NdhB, NdhC, NdhD, NdhE, NdhF, and NdhG).

the submillisecond time range. Electron transfer reactions were monitored in vitro with samples containing purified PSI, Fd, and photosynthetic complex I (Fig. 2, C and D). Single PSI turnover was triggered with a short laser flash (Fig. 2C), and subsequent electron transfer was monitored by ultraviolet-visible light absorption (see supplementary text). Submicrosecond PSI charge separation and stabilization (fig. S14) was followed by Fd reduction by the terminal [4Fe-4S] cluster of PSI, dissociation of reduced Fd (Fd$_{red}$) from PSI, and reduction of a [4Fe-4S] cluster in photosynthetic complex I by Fd$_{red}$ (Fig. 2C). The kinetics of the latter reaction were fitted to a biexponential function with rates of 245 and 1280 s^{-1} (Fig. 2C). With the conservative assumption that the slowest component (245 s^{-1}) corresponds to the association of Fd$_{red}$ to the photosynthetic complex I, we calculated a lower

limit of $k_{2FdComplexI} = 1.0 \times 10^9$ M^{-1} s^{-1} for binding. This association constant is clearly larger than values previously measured for other Fd partner proteins (*25–27*). We conclude that Fd participates in CEF via photosynthetic complex I and that Fd recruitment to complex I is very efficient.

The above analyses converge upon the hypothesis that the surface of the peripheral arm near the N6a cluster of photosynthetic complex I is responsible for Fd binding (Fig. 3A). We identified a putative Fd binding site in this region, guided by the surface charge at a tripartite interface formed by NdhK, NdhI, and NdhS (Fig. 3B). This surface area faces toward the missing [4Fe-4S] cluster N5 of the N-module of respiratory complex I (Fig. 2D).

Recent functional studies suggested that the photosynthesis-specific subunit NdhS plays an

important role in CEF of *Arabidopsis thaliana* (*22, 28*) and *Synechocystis* sp. PCC 6803 (*13*). However, because NdhS has no prosthetic group such as an Fe-S cluster or flavin, it is still elusive how it is involved in electron transfer of photosynthetic complex I. We confirmed that unbound NdhS adopts the same overall structure as in the full complex I by solving the x-ray crystal structure of recombinant NdhS at 1.90-Å resolution (table S5 and figs. S15 and S16). To assess the sites and mode of interaction between Fd and NdhS, we performed nuclear magnetic resonance (NMR) chemical shift perturbation experiments using ^{15}N-labeled Fd or NdhS with the nonlabeled counterpart, and vice versa (Fig. 3D and figs. S16 to S18). The NMR chemical shift perturbation indicated that the interaction site on NdhS was primarily located in its C-terminal region, from Glu^{104} (E104) to the C terminus, a domain that was not resolved in either the x-ray or cryo-EM structure owing to its high flexibility (Fig. 3, C and D). A similar "fly-casting" mechanism leads to fast electron transfer between Fd and ferredoxin:NADP$^+$ reductase (*25, 29*), and it might be also responsible for the fast association between Fd and photosynthetic complex I. The C-terminal segment of NdhS contains five positively charged Lys residues, which likely "catch" the negatively charged patch of Fd through an electrostatic interaction. We propose that NdhS serves as a foothold for Fd binding by tuning the binding angle of Fd toward NdhI, the catalytic subunit with a redox center next to NdhS (Fig. 3C and fig. S19), as is the case for the variable subunit of ferredoxin:thioredoxin reductase and for the PsaE subunit of PSI.

Our structure of photosynthetic complex I suggests that adaptation of modular domains and interfaces contributes to functional differences between it and homologous complexes. The minimal functional unit of the Q-module for Fd-dependent electron transfer is shared with membrane-bound hydrogenase from Archaea (*30*), thus suggesting that they also share the minimal required interaction site for Fd binding. In respiratory complex I, the N-module is attached to the Q-module to enable NADH oxidation (*21*), whereas in photosynthetic complex I, extensions and accessory subunits (including NdhS) facilitate highly efficient electron transfer from Fd. The photosynthesis-specific structural elements may also mediate supercomplex formation with PSI, which is proposed to further optimize CEF in cyanobacteria and plants (*15*).

REFERENCES AND NOTES

1. Y. Munekage *et al.*, *Nature* **429**, 579–582 (2004).
2. G. Peltier, E.-M. Aro, T. Shikanai, *Annu. Rev. Plant Biol.* **67**, 55–80 (2016).
3. N. Battchikova, M. Eisenhut, E.-M. Aro, Cyanobacterial NDH-1 complexes: Novel insights and remaining puzzles *Biochim. Biophys. Acta* **1807**, 935–944 (2011).
4. L. A. Sazanov, *Nat. Rev. Mol. Cell Biol.* **16**, 375–388 (2015).
5. J. Hirst, M. M. Roessler, Energy conversion, redox catalysis and generation of reactive oxygen species by respiratory complex I. *Biochim. Biophys. Acta* **1857**, 872–883 (2016).
6. C. Wirth, U. Brandt, C. Hunte, V. Zickermann, Structure and function of mitochondrial complex I. *Biochim. Biophys. Acta* **1857**, 902–914 (2016).

Fig. 2. Assignment of Fe-S clusters by EPR spectroscopy and in vitro electron transfer kinetics from PSI via Fd toward complex I. (**A**) [4Fe-4S] clusters N6a, N6b, and N2 with coordinating subunits NdhI (dark salmon) and NdhK (ruby) compared with the corresponding *T. thermophilus* subunits Nqo9 and Nqo6 [gray, Protein Data Bank (PDB) 4HEA (*21*)]. (**B**) An EPR spectral simulation (red dashed line) of the spectrum at 10 K (black line), along with simulated spectra for the individual components (green, blue, and pink lines) and their associated *g*-values. (**C**) Changes in flash-induced absorption at 580 nm ($\Delta A_{580\ nm}$), attributed to Fd reduction by PSI (left) and complex I reduction by Fd_{red} (right). These changes correspond to differences between signals 1, 2, and 3, recorded in three different cuvettes containing PSI, PSI-Fd, and PSI-Fd-complex I, respectively (see individual measurements in fig. S14). The left graph shows the difference between signals 2 and 1. The slow component after 0.2 ms was fitted by a single rising exponential function (black curve; rate, 1379 s^{-1}). The difference is due to oxidized Fd (Fd_{ox}) binding to PSI (which follows Fd_{red} dissociation) with a second-order rate constant of 2.8×10^8 M^{-1} s^{-1} (see materials and methods). The downward arrow corresponds to the reduction of Fd by the PSI terminal acceptor. The right graph shows the difference between signals 3 and 2. To account for the lag preceding the signal rise due to complex I reduction by Fd_{red}, the kinetics were fitted by a biexponential function with rates of 245 and 1280 s^{-1} (black curve). The upward arrow corresponds to the reduction of a [4Fe-4S] cluster in photosynthetic complex I by Fd. The PSI, Fd, and complex I concentrations were 0.08, 5.0, and 0.24 μM, respectively. (**D**) Superposition of photosynthetic complex I (green) with the *T. thermophilus* complex I [gray, PDB 4HEA (*21*)]. The N-module—which contains the NADH binding site, the flavin mononucleotide (FMN) cofactor, and the six Fe-S clusters N1a, N1b, N3, N4, N5, and N7 that transfer electrons from NADH (light blue arrows)—is missing from photosynthetic complex I. In vitro, electrons are transferred after light-induced charge separation from PSI [PDB 5ZF0 (*31*)] via Fd [PDB 5AUI (*32*)] toward the Q-module of photosynthetic complex I, as indicated by the red and dark blue arrows. The lightning bolt indicates application of a laser flash to excite PSI. PQ, plastoquinone.
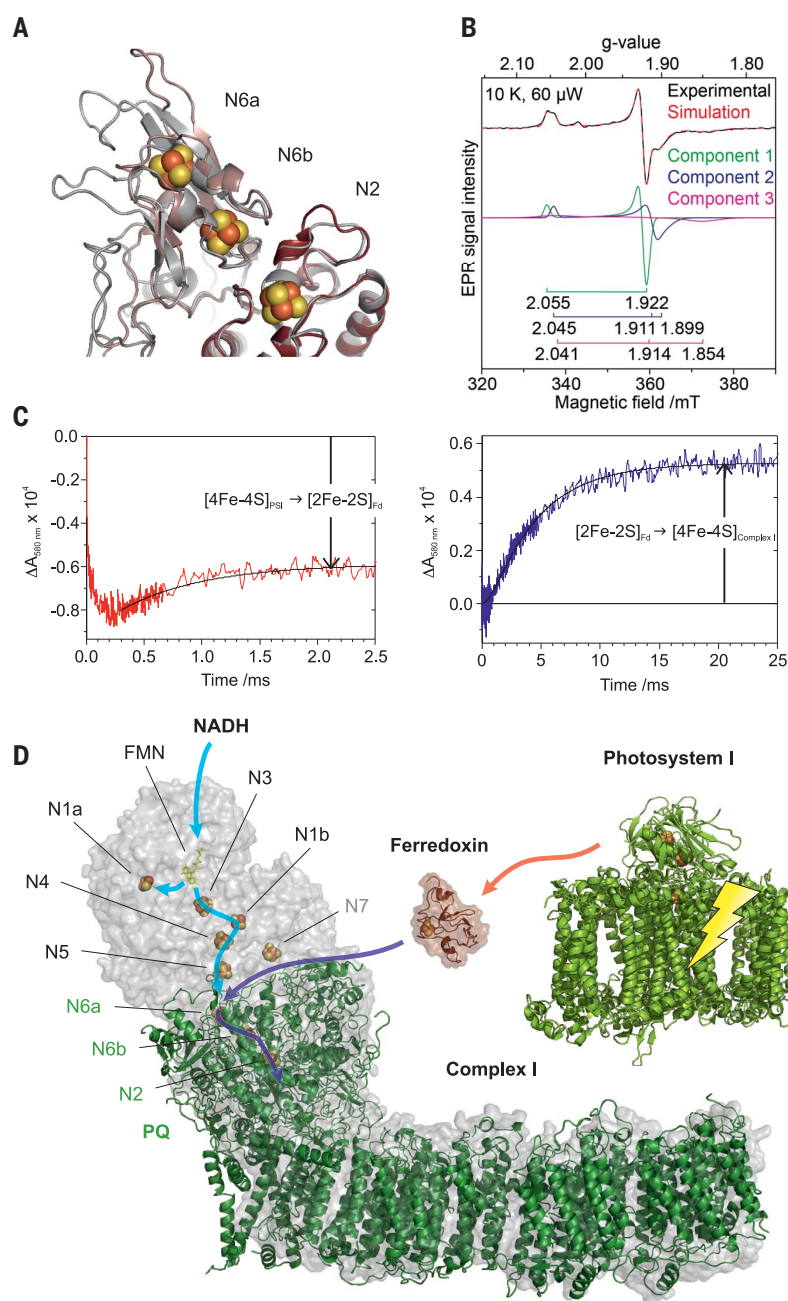

Fig. 3. Adaptation of the Q-module to Fd binding and the role of the NdhS C terminus. (**A**) Top view of the complex I surface with colored subunits. The potential Fd binding area is indicated by the yellow dashed circle. (**B**) Electrostatic potential surfaces on complex I (red for negative, white for neutral, and blue for positive) were calculated with the Adaptive Poisson-Boltzmann Solver (APBS) plug-in in PyMOL. (**C**) The C-terminal segment of NdhS (green ribbon structure) that was not resolved in the x-ray and cryo-EM structures is drawn as a dotted line in an arbitrary position. K, Lys. (**D**) Weighted ^{1}H/^{15}N chemical shift perturbations observed in [^{15}N]-NdhS upon binding to non-labeled Fd. ppm, parts per million.
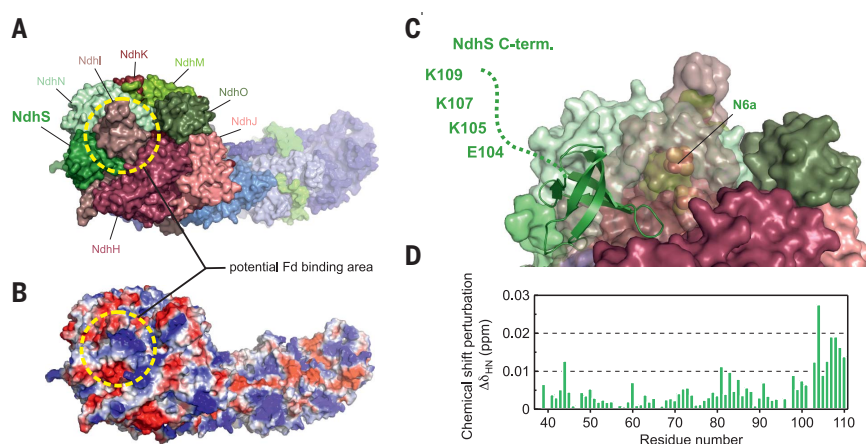
7. X. Fan, J. Zhang, W. Li, L. Peng, *Plant J.* **82**, 221–231 (2015).
8. M. M. Nowaczyk *et al.*, *Biochemistry* **50**, 1121–1124 (2011).
9. T. Ogawa, *Plant Physiol.* **99**, 1604–1608 (1992).
10. N. Battchikova, P. Zhang, S. Rudd, T. Ogawa, E.-M. Aro, *J. Biol. Chem.* **280**, 2587–2595 (2005).
11. P. Prommeenate, A. M. Lennon, C. Markert, M. Hippler, P. J. Nixon, *J. Biol. Chem.* **279**, 28165–28173 (2004).
12. D. Rumeau *et al.*, *Plant Cell* **17**, 219–232 (2005).
13. N. Battchikova *et al.*, *J. Biol. Chem.* **286**, 36992–37001 (2011).
14. T. Friedrich, K. Steinmüller, H. Weiss, *FEBS Lett.* **367**, 107–111 (1995).
15. L. Peng, H. Shimizu, T. Shikanai, *J. Biol. Chem.* **283**, 34873–34879 (2008).
16. V. R. I. Kaila, *J. R. Soc. Interface* **15**, 20170916 (2018).
17. V. Zickermann *et al.*, *Science* **347**, 44–49 (2015).
18. A. A. Agip *et al.*, *Nat. Struct. Mol. Biol.* **25**, 548–556 (2018).
19. L. A. Sazanov, *J. Bioenerg. Biomembr.* **46**, 247–253 (2014).
20. K. Fiedorczuk *et al.*, *Nature* **538**, 406–410 (2016).
21. R. Baradaran, J. M. Berrisford, G. S. Minhas, L. A. Sazanov, *Nature* **494**, 443–448 (2013).
22. H. Yamamoto, L. Peng, Y. Fukao, T. Shikanai, *Plant Cell* **23**, 1480–1493 (2011).
23. M. Narayanan *et al.*, *J. Biol. Chem.* **288**, 14310–14319 (2013).
24. T. Yano, S. Magnitsky, V. D. Sled', T. Ohnishi, T. Yagi, *J. Biol. Chem.* **274**, 28598–28605 (1999).
25. N. Cassan, B. Lagoutte, P. Sétif, *J. Biol. Chem.* **280**, 25960–25972 (2005).
26. P. Sétif *et al.*, *Biochemistry* **48**, 2828–2838 (2009).
27. A. P. Srivastava, D. B. Knaff, P. Sétif, *Biochemistry* **53**, 5092–5101 (2014).
28. H. Yamamoto, T. Shikanai, *J. Biol. Chem.* **288**, 36328–36337 (2013).
29. M. Maeda *et al.*, *Biochemistry* **44**, 10644–10653 (2005).
30. H. Yu *et al.*, *Cell* **173**, 1636–1649.e16 (2018).
31. H. Kubota-Kawai *et al.*, *Nat. Plants* **4**, 218–224 (2018).
32. R. Mutoh *et al.*, *Biochemistry* **54**, 6052–6061 (2015).

ACKNOWLEDGMENTS

SUPPLEMENTARY MATERIALS

Science

Structural adaptations of photosynthetic complex I enable ferredoxin-dependent electron transfer

Jan M. Schuller, James A. Birrell, Hideaki Tanaka, Tsuyoshi Konuma, Hannes Wulfhorst, Nicholas Cox, Sandra K. Schuller, Jacqueline Thiemann, Wolfgang Lubitz, Pierre Sétif, Takahisa Ikegami, Benjamin D. Engel, Genji Kurisu and Marc M. Nowaczyk

Plugging into the pump
Photosynthetic organisms use light to fix carbon dioxide in a process that requires both chemical reducing equivalents and adenosine triphosphate (ATP). Balancing the ratio of these inputs is accomplished by a short circuit in electron flow through photosynthetic complex I, a proton pump that contributes to ATP production but does not increase net reducing equivalents in the cell. Schuller *et al.* solved a cryo-electron microscopy structure of photosynthetic complex I (see the Perspective by Brandt) and went on to reconstitute electron transfer using the electron carrier protein ferredoxin.
Science, this issue p. 257; see also p. 230

ARTICLE TOOLS	http://science.sciencemag.org/content/363/6424/257
SUPPLEMENTARY MATERIALS	http://science.sciencemag.org/content/suppl/2018/12/19/science.aau3613.DC1
RELATED CONTENT	http://science.sciencemag.org/content/sci/363/6424/230.full
REFERENCES	This article cites 87 articles, 21 of which you can access for free http://science.sciencemag.org/content/363/6424/257#BIBL
PERMISSIONS	http://www.sciencemag.org/help/reprints-and-permissions